Yuting Chen, Abel Santos, Ye Wang, Tushar Kumeria, Daena Ho, Junsheng Li, Changhai Wang, Dusan Losic
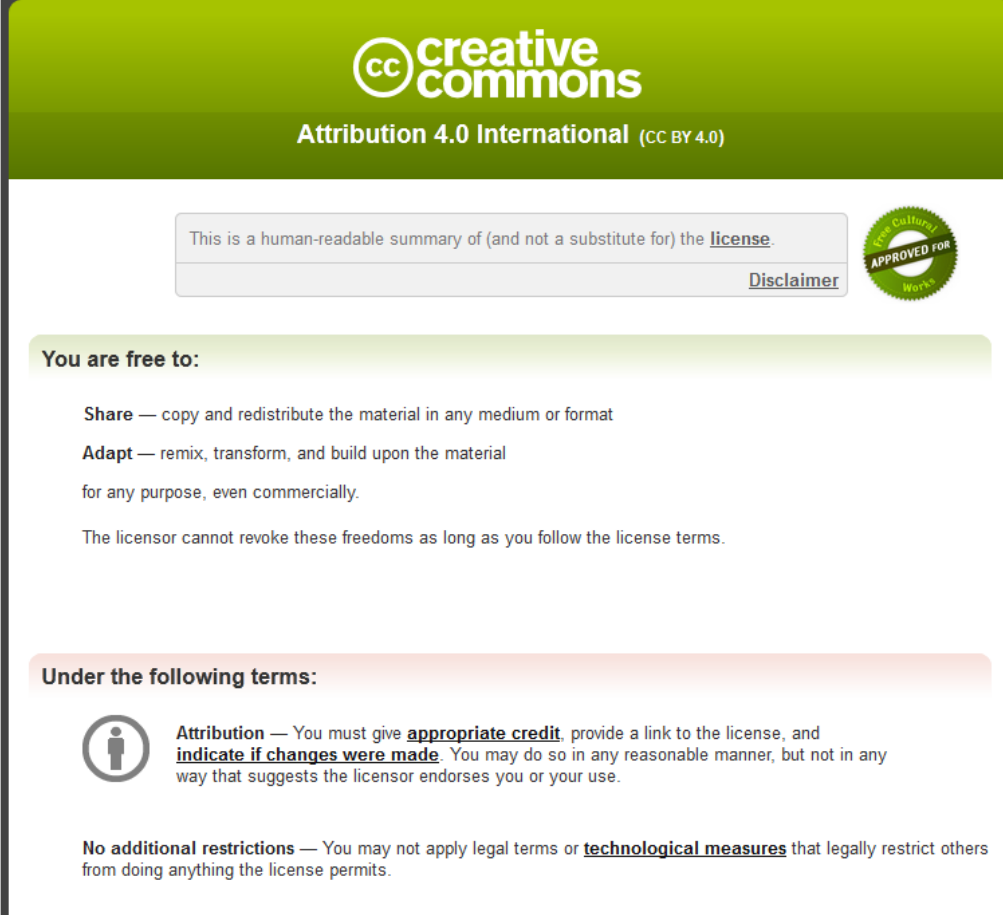**Rational design of photonic dust from nanoporous anodic alumina films: a versatile photonic nanotool for visual sensing**
Scientific Reports, 2015; 5:12893-1-12893-12

http://hdl.handle.net/2440/94214

SCIENTIFIC REP☼RTS

Rational Design of Photonic Dust from Nanoporous Anodic Alumina Films: A Versatile Photonic Nanotool for Visual Sensing

Yuting Chen[1,2,3], Abel Santos[1], Ye Wang[1], Tushar Kumeria[1], Daena Ho[1], Junsheng Li[2], Changhai Wang[3] & Dusan Losic[1]

Herein, we present a systematic study on the development, optimisation and applicability of interferometrically coloured distributed Bragg reflectors based on nanoporous anodic alumina (NAA-DBRs) in the form of films and nanoporous microparticles as visual/colorimetric analytical tools. Firstly, we synthesise a complete palette of NAA-DBRs by galvanostatic pulse anodisation approach, in which the current density is altered in a periodic fashion in order to engineer the effective medium of the resulting photonic films in depth. NAA-DBR photonic films feature vivid colours that can be tuned across the UV-visible-NIR spectrum by structural engineering. Secondly, the effective medium of the resulting photonic films is assessed systematically by visual analysis and reflectometric interference spectroscopy (RIfS) in order to establish the most optimal nanoporous platforms to develop visual/colorimetric tools. Then, we demonstrate the applicability of NAA-DBR photonic films as a chemically selective sensing platform for visual detection of mercury(II) ions. Finally, we generate a new nanomaterial, so-called photonic dust, by breaking down NAA-DBRs films into nanoporous microparticles. The resulting microparticles (μP-NAA-DBRs) display vivid colours and are sensitive towards changes in their effective medium, opening new opportunities for developing advanced photonic nanotools for a broad range of applications.

Visual/colorimetric analytical tools are outstanding alternatives to conventional diagnosis techniques based on expensive materials and complex devices. The detection principle in these analytical devices relies on colour changes, which occur in a matrix/platform when it interacts with analyte molecules[1–4]. Changes in colour are subsequently translated into quantifiable values of a given parameter (e.g. concentration of analyte, pH, temperature, etc.) by means of a previously established calibration scale (i.e. calibration curve relating parameter weight with colour change). One of the most widespread visual/colorimetric assays is the litmus paper, which makes it possible to precisely measure levels of pH in aqueous solutions by simple visual analysis[5–6]. Another outstanding example of colorimetric analytical tool is paper chromatography, which was pioneered by Mikhail S. Tswett in 1905. Originally, paper chromatography was envisaged for surveying constituents and pigments of plants by sequential separation and visual identification. These paper-based devices became the origin of a flow of studies aimed to develop paper-based bioassay platforms for diagnosis (e.g. pregnancy test strips)[7–10]. A more sophisticated variant of these analytical tools was reported in 2004 by Whitesides and co-workers, who developed POCKET, a paper-based visual/colorimetric immunoassay[11]. This study became a breakthrough in

[1]School of Chemical Engineering, The University of Adelaide, Engineering North Building, 5005 Adelaide, Australia. [2]College of Food Science and Technology, Nanjing Agricultural University, 210095 Nanjing, P. R. China. [3]Jiangsu Key Laboratory of Marine Biology, College of Resources and Environmental Science, Nanjing Agricultural University, 210095 Nanjing, P. R. China. Correspondence and requests for materials should be addressed to A.S. (email: abel.santos@adelaide.edu.au) or CW. (email: chwang@njau.edu.cn)

the field of microfluidic paper-based analytical devices (μPADs), opening new opportunities to overcome the inherent limitations of conventional analytical tools[12–16]. μPADs were envisaged for cost-competitive and easy-to-use diagnosis in developing world since these devices provide rapid analysis using small volumes of fluid and can be produced at low manufacturing costs.

Paper has become the most popular matrix/platform for developing visual/colorimetric analytical tools as a result of its superior properties (e.g. low cost, availability, capability to absorb liquids, lightweight and thin thickness, biocompatibility, strong contrast with coloured samples, flexibility and capability to be patterned/printed and chemically and physically modified, etc.)[17]. Regardless of its many advantages, paper presents some inherent limitations that prevent its use in certain applications involving high temperatures or harsh organic media conditions. In that respect, inorganic nanoporous materials such as nanoporous anodic alumina (NAA) could become a potential alternative platform for developing visual/colorimetric analytical tools for these applications since NAA can support harsh conditions of temperature and organic solvents. NAA is produced by electrochemical anodisation of aluminium substrates in acid electrolytes and its nanoporous structure can be precisely engineered by means of the anodisation parameters[18–22]. NAA presents excellent chemical, mechanical and physical stability, can be produced at industrial scale through a cost-competitive fabrication process, has stable optical signals without additional passivation steps, its nanoporous structure is versatile and controllable, can be chemically modified by well-established functionalisation protocols and patterned by lithographic techniques[23,24]. In addition, NAA is an outstanding optical material, the nanoporous structure of which can be precisely engineered to guide, reflect, transmit, emit and enhance incident light[25–35]. Despite these advantages, typically NAA displays transparent colour, which has prevented its applicability for visual/colorimetric sensing applications. Recently, some electrochemical approaches have made it possible to produce interferometrically coloured NAA films by structural engineering of its nanoporous structure[36]. This nanomaterial, so-called coloured aluminum, is composed of a stack of layers of NAA featuring periodic increments and decrements of porosity in depth. These nanoporous photonic structures, which resemble natural structures present in coloured butterflies and beetles, can be approximated to distributed Bragg reflectors (NAA-DBRs) and can be precisely engineered to selectively reflect light at specific wavelengths within the UV-visible-NIR spectrum[37–40]. Therefore, NAA-DBRs can be produced featuring a broad range of vivid colours across the UV-visible-NIR spectrum by engineering their nanoporous structure through the anodisation parameters. Furthermore, as a result of their optical properties, NAA-DBR photonic films experience sharp blue/red shifts in colour when their effective medium is altered. This property could be readily used to develop new visual/colorimetric analytical tools for detecting analytes. Surprisingly, the potential use of NAA-DBR photonic films as a matrix/platform for developing visual/colorimetric analytical tools has hitherto been neglected.

In this scenario, we present for the first time a systematic study on the development, optimisation and applicability of coloured NAA-DBRs for visual/colorimetric analytical tools in the form of films and nanoporous microparticles. Firstly, we produce a complete palette of NAA-DBR photonic films featuring vivid colours within the UV-visible-NIR spectrum by structural engineering. Secondly, the effective medium of the resulting photonic films is assessed systematically by visual analysis and reflectometric interference spectroscopy in order to establish the most optimal nanoporous platform to develop visual/colorimetric tools. Finally, we demonstrate the applicability of NAA-DBR photonic films in the form of films and microparticles as a chemically selective photonic sensing platform for colorimetric quantification of analytes.

Results

Fabrication of a complete palette of NAA-DBR photonic films by pulse anodisation. NAA-DBR films were produced by anodising aluminium (Al) foils through a pulse anodisation approach under current density control in an aqueous solution 1.1 M of sulphuric acid (H$_2$SO$_4$). Prior to anodisation, aluminium substrates were electropolished in a mixture of ethanol (EtOH) and perchloric acid (HClO$_4$) 4:1 (v:v) at 20 V and 5 °C for 3 min. Next, electropolished Al substrates were first anodised in 1.1 M H$_2$SO$_4$ for 1 h at a constant current density of 1.12 mA cm^{-2} to enable a homogeneous growth of the oxide layer. Subsequently, the anodisation process was switched to pulse mode, which consisted of a series of current density pulses between high (J_{high} = 1.12 mA cm^{-2}) and low (J_{low} = 0.28 mA cm^{-2}) levels for a total of 150 pulses. To generate a complete palette of coloured NAA-DBRs films, the length of the current density pulse period (T_p) and the anodisation temperature (T_{an}) were each set to four (i.e. T_p – 675, 900, 1035 and 1170 s) and three (T_{an} – 3, 1 and –1 °C) values, respectively. In our study, T_p was defined as the total time length of high (t_{high}) and low (t_{low}) anodisation current density pulses (**Equation** 1):

$$T_p = t_{high} + t_{low} \tag{1}$$

Note that, to fabricate NAA-DBRs at –1 °C and prevent the electrolyte solution from freezing at temperatures below 0 °C, the electrolyte solution was modified with 25 v% of EtOH[41–43]. Table 1 summarises the fabrication characteristics of the different NAA-DBRs produced in this study and Fig. 1a depicts an illustration describing the electrochemical approach used to engineer the structure of NAA and generate a complete palette of coloured aluminium based on NAA-DBRs.

T_p (s)	T_{an} (°C)		
	3	1	−1
675	NAA-DBR$_{(675;3°C)}$	NAA-DBR$_{(675;1°C)}$	NAA-DBR$_{(675;−1°C)}$
900	NAA-DBR$_{(900;3°C)}$	NAA-DBR$_{(900;1°C)}$	NAA-DBR$_{(900;−1°C)}$
1035	NAA-DBR$_{(1035;3°C)}$	NAA-DBR$_{(1035;1°C)}$	NAA-DBR$_{(1035;−1°C)}$
1170	NAA-DBR$_{(1170;3°C)}$	NAA-DBR$_{(1170;1°C)}$	NAA-DBR$_{(1170;−1°C)}$

Table 1. NAA-DBR photonic films produced in this study as a function of the fabrication conditions (i.e. T_p and T_{an}).

The nanoporous structure of NAA-DBRs can be described as a stack of nanoporous layers featuring high and low levels of porosity sequentially alternated. Figure 1b shows a schematic illustration of the structure of NAA-DBR photonic films produced in this study, which can be defined by the total length of the film (L_T), the lengths of the segments with low (L_{low}) and high (L_{high}) porosity and the period length ($L_{Tp} = L_{low} + L_{high}$). Galvanostatic pulse anodisation makes it possible to engineer the effective refractive index of NAA in depth by switching the level of porosity through the current density in the course of the anodisation process. In other words, the anodisation profile is translated into layers of high ($n_{eff-high}$) and low ($n_{eff-low}$) effective refractive index (i.e. low (J_{low}) and high (J_{high}) current density, respectively). Therefore, a rational design of the anodisation profile enables a precise control over the interaction between light and matter in NAA, making it achievable to produce a variety of photonic nanostructures such as NAA-DBRs. Under certain anodisation conditions, NAA-DBRs can display vivid colours, which can be tuned across the UV-visible-NIR spectrum. In our study, we modified two anodisation parameters in order to produce a complete palette of photonically coloured NAA-DBR films (Fig. 1c). While the anodisation period was set to four different values (675, 900, 1035 and 1170 s), the anodisation temperature was set to three values (3, 1 and −1 °C). Note that the proportion between the time length of high and low anodisation current density pulses was kept at 1:4 ($t_{high}:t_{low}$) throughout the above-mentioned experiments. Figure 1a shows a representative example of anodisation profile used in our study describing the different characteristic parameters and Fig. 1d depicts representative SEM images of the resulting NAA-DBR films. These biomimetic photonic nanostructures are similar to natural photonic structures present in organisms such as butterflies, beetles and birds[37–40]. In these photonic coatings, colour is generated by the interaction light-matter, without the presence of any pigment.

Figure 2a illustrates digital images of the NAA-DBR photonic films produced in our study by modifying T_p and T_{an}. These demonstrate that NAA-DBRs can be produced with a broad range of vivid colours, including gold, brown, pink, purple, blue, green and yellow. Note that the wavelength of the light reflected by the NAA-DBR structure ($\lambda_{reflection}$) can be tuned across the UV-visible-NIR spectrum by engineering its nanoporous structure through the anodisation parameters, in this case T_p and T_{an} (Fig. 2b).

The Bragg's law adapted to NAA-based distributed Bragg reflectors is given by Equation 2:

$$\lambda_{reflection} = 2\left(L_{high} n_{eff-low} + L_{Low} n_{eff-high}\right) \tag{2}$$

Therefore, NAA-DBR photonic films reflect light at longer wavelengths ($\lambda_{reflection}$) (i.e. red shift) when T_p is increased since $\uparrow T_p \rightarrow \uparrow L_{Tp} \rightarrow \uparrow(L_{high} + L_{low}) \rightarrow \uparrow\lambda_{reflection}$. This red shift can be further increased by decreasing the anodisation temperature as the porosity level in NAA decreases with T_{an} and $\downarrow T_{an} \rightarrow (\uparrow n_{eff-high}$ and $\uparrow n_{eff-low}) \rightarrow \uparrow\lambda_{reflection}$. This enables the selective design of colour of NAA-DBRs across the UV-visible-NIR spectrum by two anodisation parameters.

Assessment of the effective medium of NAA-DBR photonic films as a visual sensing tool.

The optical properties of NAA-DBR films were systematically assessed by different approaches in order to demonstrate their applicability as visual sensing tools. First, visual analysis of colour change after partial infiltration of the nanoporous structure of NAA-DBRs with ethanol (EtOH) was performed. In this analysis, half sample was coated with a transparent tape in order to avoid total infiltration with EtOH and obtain a better visual contrast between infiltrated and non-infiltrated structure. This analysis was further extended by measuring changes in the effective optical thickness (ΔOT_{eff}) of these photonic films by reflectometric interference spectroscopy (RIfS)[23,24]. Note that ΔOT_{eff} was estimated by the Fabry–Pérot relationship (Equation 3):

$$OT_{eff} = 2n_{eff}L_T \tag{3}$$

where OT_{eff} is the effective optical thickness of the film, n_{eff} is its effective refractive index and L_T is its physical thickness.

NAA-DBR films undergo sharp colour changes when their effective medium is altered. For instance, filling the nanopores of NAA-DBR films with ethanol (i.e. $n_{ethanol} = 1.362$ RIU), which is a medium with higher refractive index than air (i.e. $n_{air} = 1$ RIU), produces a red shift in their characteristic colour
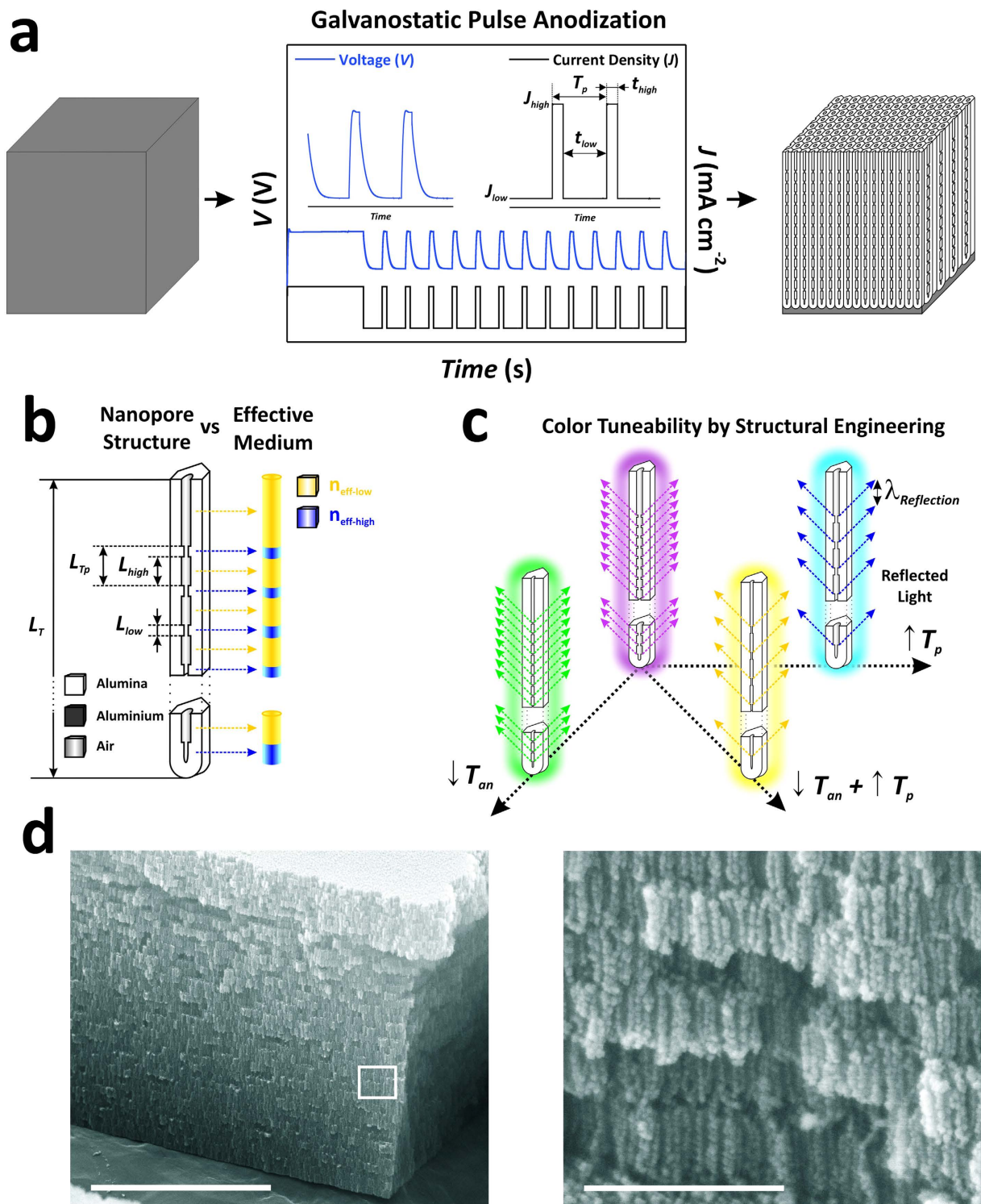
Figure 1. Structural engineering of NAA-DBR photonic films by galvanostatic pulse anodisation.
(**a**) Schematic illustration describing how the structure of NAA-DBRs is engineered in depth by galvanostatic pulse anodisation and example of anodisation profile describing the characteristic fabrication parameters (i.e. J_{high}, J_{low}, t_{high} and t_{low}). (**b**) Illustration depicting the most representative geometric features in NAA-DBR photonic films (i.e. L_T, L_{Tp}, L_{high} and L_{low}) and their direct relationship with the effective medium of NAA-DBRs. (**c**) Schematic illustration showing how color in NAA-DBRs can be tuned across the UV-visible-NIR spectrum by the anodisation parameters (i.e. T_p and T_{an}). (**d**) Cross-section SEM images of NAA-DBRs (left—general view (scale bar = 5 μM) and right—magnified view of white rectangle shown in left (scale bar = 500 nm)).
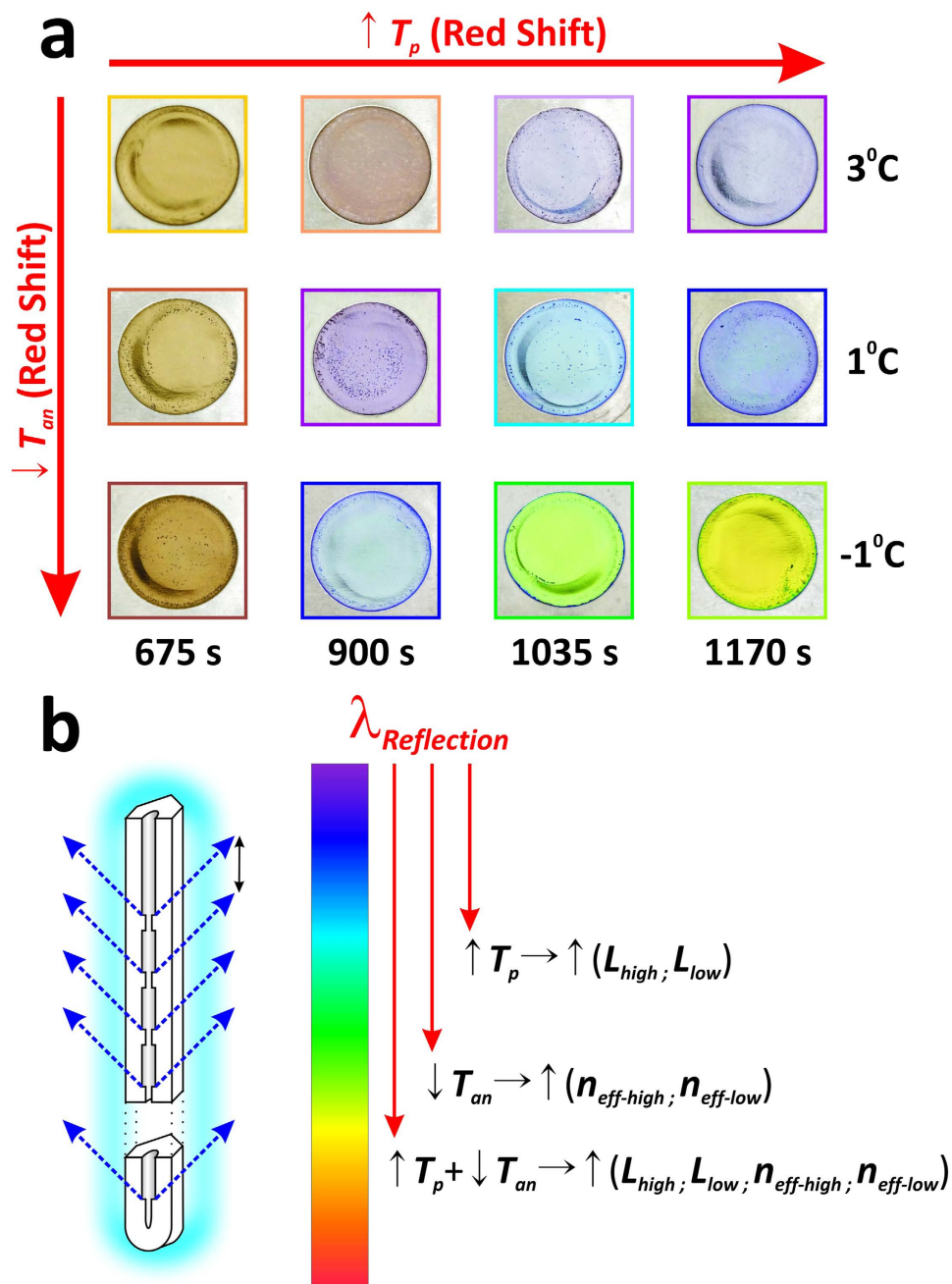
Figure 2. Colour tuneability in NAA-DBRs. (**a**) Digital pictures of NAA-DBR photonic films produced in this study by modifying T_p and T_{an} (NB: aluminium substrates were electrochemically anodised through a circular window of 1 cm in diameter). (**b**) Schematic illustration showing how the different fabrication parameters make it possible to tune the colour of the resulting NAA-DBR film across the UV-visible-NIR spectrum by engineering the interaction light-matter.

(Fig. 3a). This property can be readily used to develop visual sensing tools for a broad range of applications. Surprisingly, to the best of our knowledge, so far no studies have explored the potential of NAA-DBRs as photonic platforms for colorimetric sensing. Figure 3b displays a set of digital pictures of the different NAA-DBRs produced in this study after selective infiltration of their nanoporous structure with EtOH. This analysis reveals that some NAA-DBR films are potential candidates for developing colorimetric sensing tools as they experience sharp colour changes after infiltration. Our visual analysis establishes that the most suitable NAA-DBRs for this application are NAA-DBR$_{(900s;-1\,°C)}$, NAA-DBR$_{(1035s;3\,°C)}$, NAA-DBR$_{(1035s;1\,°C)}$, NAA-DBR$_{(1035s;-1\,°C)}$, NAA-DBR$_{(1170s;3\,°C)}$, NAA-DBR$_{(1170s;1\,°C)}$ and NAA-DBR$_{(1170s;-1\,°C)}$. In order to gain a more objective insight into the most sensitive NAA-DBR film, we quantified the effective optical thickness change by RIfS after infiltration of these photonic nanostructures with EtOH. Figure S1 (Supporting Information) shows several examples of real-time monitoring of ΔOT_{eff} by RIfS.
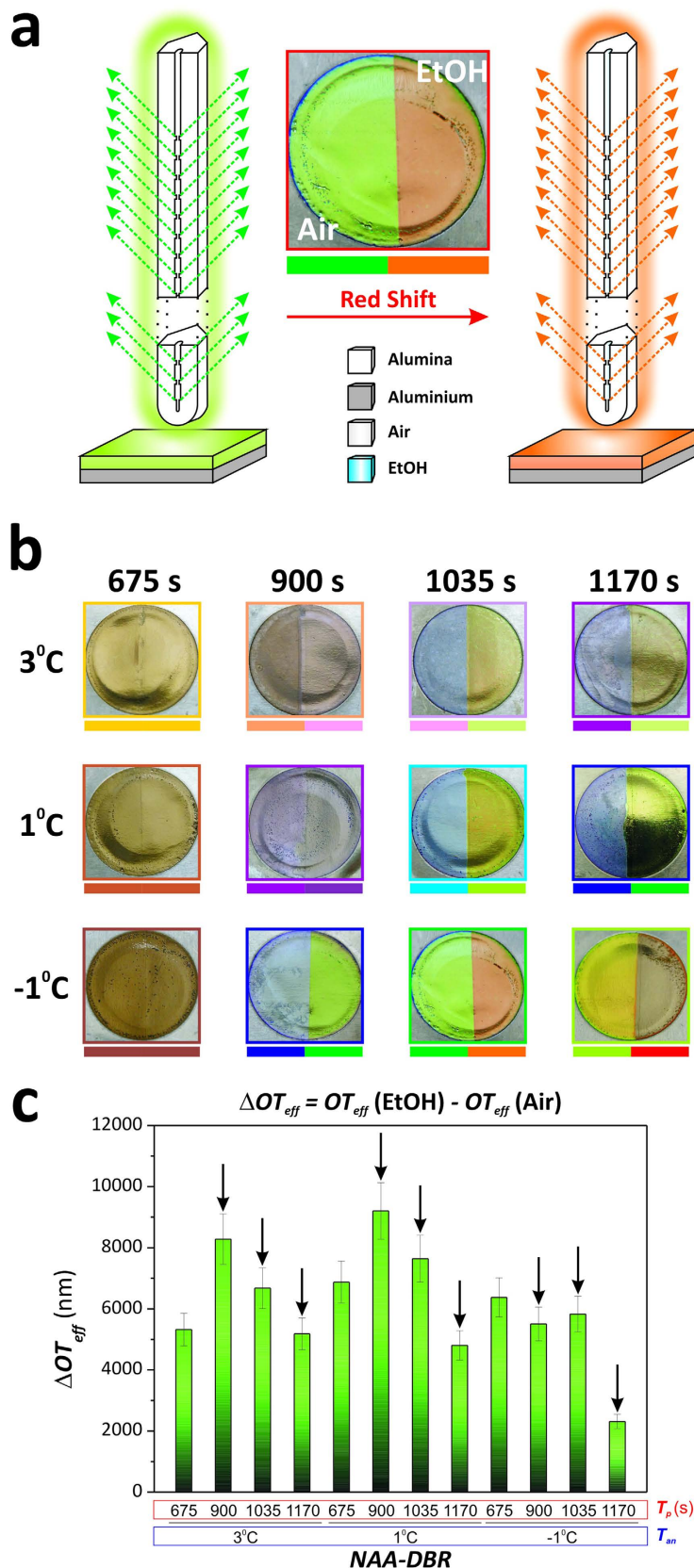
Figure 3. Optical assessment of NAA-DBR photonic films as visual/colorimetric tool. (**a**) Schematic illustration describing how the effective medium change is translated into a colour change in NAA-DBRs. (**b**) Digital pictures of NAA-DBRs after partial infiltration of their structure with EtOH. (**c**) ΔOT_{eff} measured by RIfS after infiltration of the nanoporous structure of NAA-DBRs with EtOH (black arrows denote NAA-DBRs that experience a visible change in colour after infiltration).
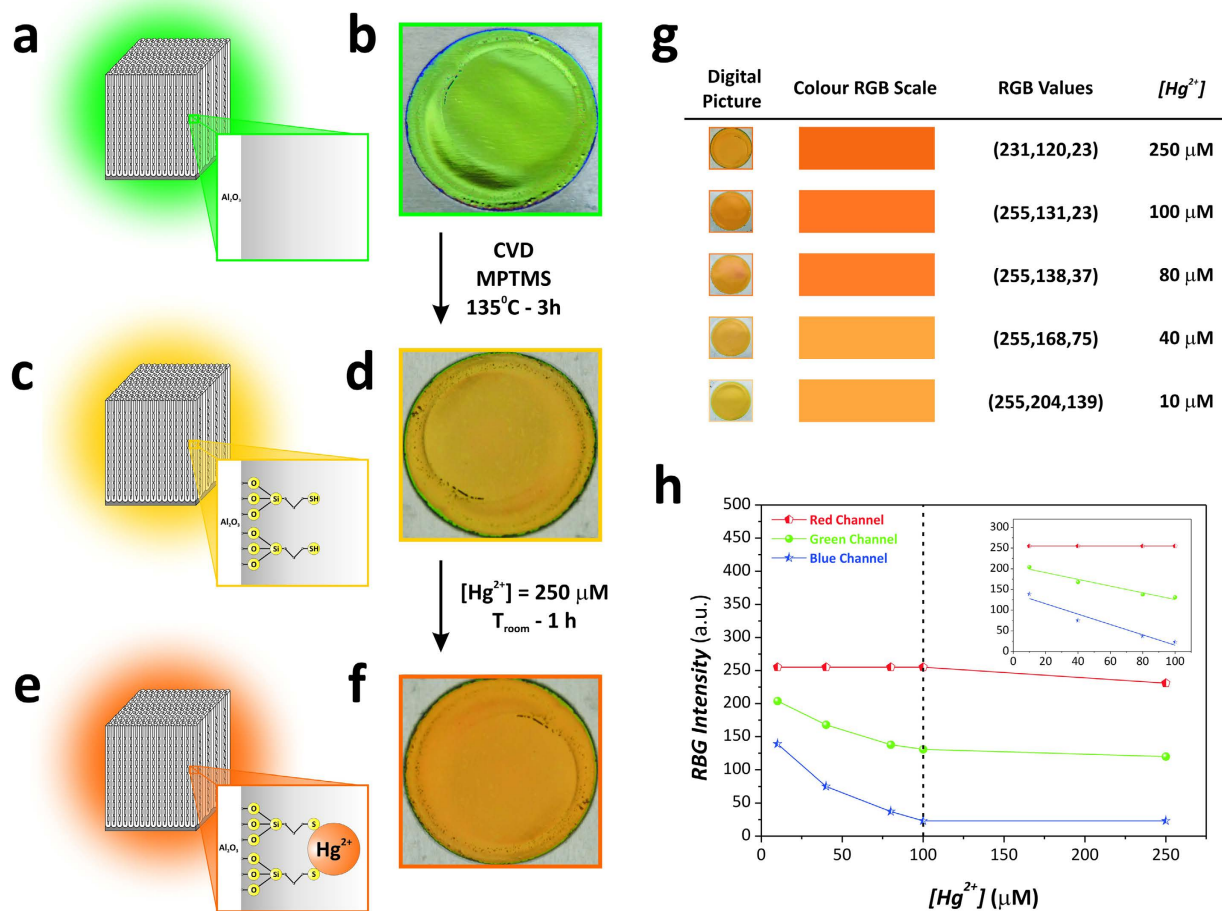
Figure 4. NAA-DBR photonic films as colorimetric tools to detect mercury ions in aqueous samples.
Schematic illustrations and digital pictures of a NAA-DBR type NAA-DBR$_{(1035s;-1°C)}$ as-produced (**a–b/**
green), after chemical functionalisation with MPTMS via chemical vapour deposition (**c–d**/dark yellow)
and after immersion in an aqueous solution 250 μM Hg^{+2} (**e-f**/orange). (**g**) Table summary showing digital
pictures, RGB colours and values of MPTMS-functionalised NAA-DBRs exposed to different concentrations
of mercury ions. (**h**) Decomposition of RGB colours in R—Red Channel, G—Green Channel and B—Blue
Channel signals as a function of the analyte concentration (inset displays the linear working range for G and
B channels, which was found to be from 10 to 100 μM).

Figure 3c and Table S1 summarise the obtained results, which demonstrates that the most sensitive effective medium is given by the structure NAA-DBR$_{(900s;1°C)}$. Nevertheless, as the digital pictures reveal, this NAA-DBR is not suitable for visual sensing. Among those NAA-DBRs displaying sharp changes in colour after infiltration (i.e. black arrows in Fig. 3c), NAA-DBR$_{(1035s;1°C)}$ presents the highest effective optical thickness change after infiltration with a medium of higher refractive index. Motivated by these results, we decided to explore the potential of NAA-DBRs as chemically selective visual sensing platforms.

NAA-DBR photonic films for visual detection of mercury ions. Mercury(II) ions (Hg^{2+}) are the largest mercuric pollutants in environmental water and sources must be monitored throughout. These heavy metal ions can produce genetic mutations in developing embryos and damage the immune and nervous systems and affect motion coordination, touch, taste and sight in adults[28]. Therefore, to develop ultra-sensitive, handy and cost-competitive visual sensors with the ability to establish levels of mercuric pollutants in water sources is a must. As a proof-of-concept, we functionalised the surface of a set of NAA-DBR films type NAA-DBR$_{(1035s;-1°C)}$ with thiol groups (-SH) in order to demonstrate the ability of these photonic nanostructures to detect levels of Hg^{2+} in water by simple visual analysis. As Fig. 4 shows, these photonic films undergo a sharp change in colour from green (Fig. 4a,b) to dark yellow (Fig. 4d,e) after functionalisation with 3-(mercaptopropyl)-trimethoxysilane (MPTMS) and from dark yellow to orange (Fig. 4e,f) after exposure to an aqueous solution 250 μM Hg^{+2}. Motivated by these results, we decided to further explore the potential of NAA-DBRs as a visual sensing tool for the quantitative

detection of mercury ions. To this end, MPTMS-functionalised NAA-DBRs type NAA-DBR$_{(1035s;-1°C)}$ were exposed to different analyte solutions of Hg^{+2} (i.e. 10, 40, 80, 100 and 250 μM). The obtained results, which are summarised in Fig. 4g, reveal that there is a direct correlation between the colour of NAA-DBRs and the concentration of analyte. Image analysis of digital pictures of these samples made it possible to decompose the colour of NAA-DBRs into RGB scale components and thus to relate the analyte concentration with the colour intensity for each of these channels (i.e. R—Red Channel, G—Green Channel and B—Blue Channel) (Fig. 4h). At first glance it was observed that, while the red channel was saturated at any of the different concentrations of mercury ions (i.e. 255 a.u.—maximum intensity), the green and blue channels presented a direct correlation with the analyte concentration from 10 to 100 μM. A linear fitting within that working range allowed us to establish the sensing performance of each channel (inset in Fig. 4h). Channels G and B achieved a sensitivity of 0.81 ± 0.11 a.u. μM^{-1} and 1.25 ± 0.21 a.u. μM^{-1}, a low limit of detection of 29.4 μM and 37.3 μM, with a linearity (R^2) of 0.9494 and 0.9202, respectively. These promising results demonstrate that NAA-DBRs are suitable platforms to develop colorimetric tools to detect heavy metal ions.

NAA-DBR photonic dust for visual sensing.   To explore the versatility of NAA-DBR photonic nanostructures as sensing nanotools, NAA-DBR films were broken down into nanoporous microparticles by sonication (Fig. 5a). Figures 5b–g compile a set of representative SEM and optical microscopy images of the microporous particles produced from NAA-DBR photonic films (μP-NAA-DBRs), which feature an average size of 43.2 ± 7.5 μM. These nanoporous microparticles can be massively produced from NAA-DBR films (Fig. 5b) and feature a narrow size distribution, which can be tuned by the sonication treatment (Fig. 5c). Furthermore, as optical microscopy reveals (Fig. 5d–g), these photonic structures keep the optical properties of the original films: namely; i) display vivid bright colours across the UV-visible-NIR spectrum, which can be tuned by a rational design of the anodisation process and ii) undergo colour changes when the effective medium of the μP-NAA-DBR is altered (Fig. 5h). Figure 5i demonstrates that μP-NAA-DBRs experience sharp changes in colour when their effective medium is filled with isopropanol (IPA–$n_{isopropanol}$ = 1.378 RIU) and recover the original colour when IPA evaporates. For instance, μP-NAA-DBRs obtained from NAA-DBR films type NAA-DBR$_{(1035s;1°C)}$ and NAA-DBR$_{(1035s;-1°C)}$ display green and red colour, respectively, when they are immersed in IPA (i.e. left column NAA-DBR$_{(1035s;1°C)}$ and right column NAA-DBR$_{(1035s;-1°C)}$). These μP-NAA-DBRs recover their original colour when IPA is evaporated after 2 min (see **Videos S1 and S2**—Supporting Information).

Previous studies have reported on similar approaches used to produce porous silicon photonic microparticles[44–47]. This photonic material, so-called photonic dust, has been demonstrated as an outstanding visual/colorimetric nanotool for a broad range of applications. However, our study is the first report on photonic dust based on NAA. These photonic nanoporous microparticles have a promising potential to be employed in high-throughput screening applications (e.g. multiplexed detection of DNA oligonucleotides)[48], sensors[49], self-reporting drug delivery carriers[50], encoded tracers and tags for products[46].

Discussion

This study has reported on a rationally designed electrochemical approach aimed to generate a complete palette of nanoporous anodic alumina distributed Bragg reflectors. NAA-DBRs produced by galvanostatic pulse anodisation in sulphuric acid electrolyte display vivid colours, which can be tuned across the UV-visible-NIR spectrum by the anodisation parameters. These photonic films are highly sensitive structures that undergo sharp changes in colour when their effective medium is altered. Motivated by this outstanding property, we systematically explored different approaches to demonstrate the applicability of NAA-DBRs as visual/colorimetric photonic tools. First, we established the most suitable NAA-DBR films for visual sensing by selective infiltration of their nanoporous structure with ethanol. This analysis was further validated by measuring changes in the effective optical thickness of these photonic films by RIfS. Then, we demonstrated that NAA-DBR films can be used as a sensing tool to detect and quantify mercury ions in a chemically selective manner by simple visual analysis and image analysis. Finally, we produced for the first time a new photonic nanomaterial based on μP-NAA-DBRs, so-called photonic dust. μP-NAA-DBRs experience observable changes in colour when their effective medium is altered. The properties of μP-NAA-DBRs can be precisely designed by the anodisation parameters, enabling new opportunities to produce advanced sensing nanotools for a broad range of analytes and applications, including high-throughput biological and chemical screening, monitoring of environmental pollutants, photonic tags and tracers and UV protective films and paints.

Methods

Materials.   Aluminium foils of high purity (99.9997%) and 0.32 mm thick were supplied by Goodfellow Cambridge Ltd. (UK). Sulphuric acid (H_2SO_4), perchloric acid ($HClO_4$), chromium trioxide (CrO_3), phosphoric acid (H_3PO_4), hydrochloric acid (HCl), cupric chloride ($CuCl_2$), mercury(II) chloride ($HgCl_2$), ethanol (C_2H_5OH–EtOH), isopropanol (C_3H_8O–IPA), 3-(mercaptopropyl)-trimethoxysilane (MPTMS) and hydrogen peroxide (H_2O_2) were purchased from Sigma-Aldrich (Australia) and used as-received. The aqueous solutions used in this study were prepared with ultrapure water Option Q–Purelabs (Australia).
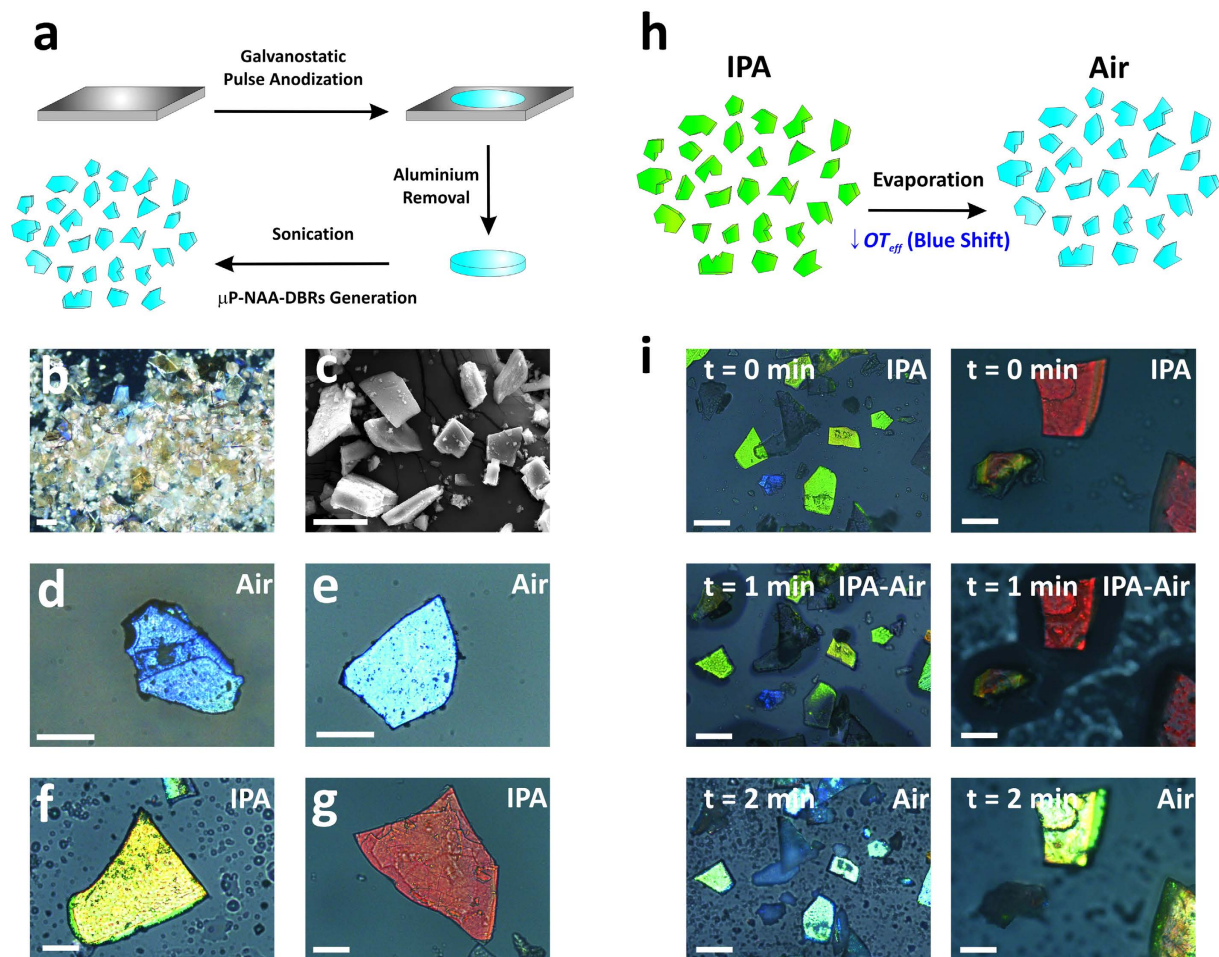
Figure 5. Photonic nanoporous microparticles obtained from NAA-DBR photonic films. (**a**) Fabrication process of μP-NAA-DBRs by breaking down NAA-DBR films into microparticles *via* sonication. (**b**) Optical microscopy image (natural illumination) of μP-NAA-DBRs showing how these microparticles can be massively produced from NAA-DBR films (scale bar 100 μm). (**c**) SEM image of μP-NAA-DBRs showing the morphology of this photonic material, which can be produced with a narrow size distribution by adjusting the sonication parameters (scale bar = 50 μm). (**d–e**) Optical microscopy images of different μP-NAA-DBRs in air (d-e) and IPA (**f–g**) (scale bars = 50 μm). (**h**) Schematic illustration of the sensing principle (i.e. colour change) in μP-NAA-DBRs based on changes in their effective medium. (**i**) Optical microscopy images extracted from videos S1 and S2 (Supporting Information), demonstrating how μP-NAA-DBRs can be used as photonic sensing tools to detect analytes by colorimetry (scale bars = 50 μm) (left column—μP-NAA-DBR$_{(1035s;1°C)}$ and right column—μP-NAA-DBR$_{(1035s;-1°C)}$).

Evaluation of coloured NAA-DBRs films as platforms for visual sensing. The effective optical thickness changes in NAA-DBRs were monitored in real-time using a RIfS system composed of a bifurcated optical probe focusing white light from a source (LS-1LL, Ocean Optics, USA) on the surface of NAA-DBRs. The reflected light was collected by the collection fibre assembled in the same optical probe and automatically transferred to a miniature spectrometer (USB4000 + VIS-NIR-ES, Ocean Optics, USA). UV-visible optical spectra were acquired from 400 to 1000 nm and saved at intervals of 10 s, with an integration time of 10 ms and 10 average measurements. RIfS spectra were processed in Igor Pro library (Wavemetrics, USA) in order to estimate ΔOT_{eff}.

Visual/colorimetric sensing of mercury (II) ions. The capability of NAA-DBR photonic films as chemically selective and quantitative visual sensing platforms was demonstrated by modifying the surface chemistry of NAA-DBR films with MPTMS via chemical vapour deposition[51]. MPTMS molecules have a thiol terminal (-SH), which is a functional group with chemical affinity towards mercury(II) ions (Hg^{2+})[28]. In this process, NAA-DBR photonic films were first hydroxylated by immersion in boiling H_2O_2 30 wt% for 10 min at 90 °C. Then, the inner surface of NAA-DBRs was coated with a monolayer of MPTMS molecules by chemical vapour deposition. This process was performed under vacuum at 135 °C

for 3 h. Next, MPTMS-modified NAA-DBRs were washed thoroughly with ethanol and water in order to remove physisorbed MPTMS molecules. Different aqueous solutions of Hg^{2+} ions were prepared by dilution of $HgCl_2$ in ultrapure water (i.e. 10, 40, 80, 100 and 250 μM). These solutions were subsequently used to assess the sensing performance of NAA-DBR films for visual quantitative detection of mercury ions by simple immersion of MPTMS-functionalised NAA-DBRs. The binding of Hg^{2+} ions with thiol functional groups present on the inner surface of MPTMS-modified NAA-DBRs produced a sharp change in colour in these photonic films. Finally, NAA-DBRs were thoroughly washed with water to remove physisorbed Hg^{2+} ions and reveal the actual colour change associated with specific immobilisation of Hg^{2+} ions. RGB colour scales were established by image analysis of digital pictures of NAA-DBRs after exposure to analyte solutions containing controlled concentrations of mercury ions. The plugin Measure RGB in ImageJ (public domain program developed at the RSB of the NIH) was used for SEM image analysis to establish the RGB values of each sample[52]. Digital images of NAA-DBRs were acquired by a mobile phone Sony Xperia™ Z3 Compact equipped with a camera of 20.7 MP (5248 × 3936 pixels) and autofocus function.

Fabrication of nanoporous photonic microparticles from NAA-DBR films. To prepare nanoporous photonic microparticles (μP-NAA-DBRs) from NAA-DBRs films, the remaining aluminium substrate was dissolved by selective wet chemical etching in a saturated solution of $HCl/CuCl_2$. Then, NAA-DBRs films were broken down into photonic microparticles by sonication in water. The resulting μP-NAA-DBRs were collected by centrifugation at 14.000 rpm for 10 min and drying at 50 °C overnight. The photonic properties of μP-NAA-DBRs in air and IPA were assessed by optical microscopy (Nikon LV100 POL optical petrographic microscope).

Structural Characterisation. The nanoporous structure of NAA-DBRs films and μP-NAA-DBRs were characterised by field emission gun scanning electron microscopy (FEG-SEM FEI Quanta 450). ImageJ was used for SEM image analysis[52].

The above-mentioned experiments were repeated three times with freshly prepared samples and solutions and the obtained values of the different experimental parameters were calculated as averages and standard deviations.

References

1. Elghanian, R., Storhoff, J. J., Mucic, R. C., Letsinger, R. L. & Mirkin, C. A. Selective colorimetric detection of polynucleotides based on the distance-dependent optical properties of gold nanoparticles. *Science* **277,** 1078–1081 (1997).
2. Rakow, N. A. & Suslick, K. S. A colorimetric sensor array for odour visualization. *Nature* **406,** 710–713 (2000).
3. Kim, J. M., Ji, E. K., Woo, S. M., Lee, H. & Ahn, D. J. Immobilized polydiacetylene vesicles on solid substrates for use as chemosensors. *Adv. Mater.* **15,** 1118–1121 (2003).
4. Liu, J. & Lu, Y. A colorimetric lead biosensor using DNAzyme-directed assembly of gold nanoparticles. *J. Am. Chem. Soc.* **125,** 6642–6643 (2003).
5. Rice, E. Laboratory preparation of litmus paper. *Ind. Eng. Chem.* **4,** 229 (1912).
6. Walpole, G. S. The use of litmus paper as a quantitative indicator of reaction. *Biochem. J.* **7,** 260–267 (1913).
7. Toennies, G. & Kolb, J. J. Techniques and reagents for paper chromatography. *Anal. Chem.* **23,** 823–826 (1951).
8. Barton, G. M., Evans, R. S. & Gardner, J. A. F. Paper chromatography of phenolic substances. *Nature* **170,** 249–250 (1952).
9. Hiscox, E. R. & Berridge, N. J. The use of paper partition chromatography in the identification of the volatile fatty acids. *Nature* **166,** 522 (1950).
10. Rydon, H. N. & Smith, P. W. G. A new method for the detection of peptides and similar compounds on paper chromatograms. *Nature* **169,** 922–923 (1952).
11. Sia, S. K., Linder, V., Parviz, B. A., Siegel, A. & Whitesides, G. M. An integrated approach to a portable and low-cost immunoassay for resource-poor settings. *Angew. Chem. Int. Ed.* **43,** 498–502 (2004).
12. Carrilho, E., Phillips, S. T., Vella, S. J., Martinez, A. W. & Whitesides, G. M. Paper microzone plates. *Anal. Chem.* **81,** 5990–5998 (2009).
13. Pollock, N. R. *et al.* A paper-based multiplexed transaminase test for low-cost, point-of-care liver function testing. *Sci. Transl. Med.* **4,** 152ra129 (2012).
14. Maxwell, E. J., Mazzeo, A. D. & Whitesides, G. M. Paper-based electroanalytical devices for accessible diagnostic testing. *MRS Bull.* **38,** 309–314 (2013).
15. Martinez, A. W. *et al.* Simple telemedicine for developing regions: Camera phones and paper-based microfluidic devices for real-time, off-site diagnosis. *Anal. Chem.* **80,** 3699–3707 (2008).
16. Martinez, A. W., Phillips, S. T. & Whitesides, G. M. Three-dimensional microfluidic devices fabricated in layered paper and tape. *Proc. Natl. Acad. Sci. USA.* **105,** 19606–19611 (2008).
17. Martinez, A. W., Phillips, S. T. & Whitesides, G. M. Diagnostics for the developing world: Microfluidic paper-based analytical devices. *Anal. Chem.* **82,** 3–10 (2010).
18. Masuda, H. & Fukuda, K. Ordered metal nanohole arrays made by a two-step replication of honeycomb structures of anodic alumina. *Science* **268,** 1466–1468 (1995).
19. Masuda, H. & Hasegwa, F. J. Self-ordering of cell arrangement of anodic porous alumina formed in sulfuric acid solution. *J. Electrochem. Soc.* **144,** L127–L130 (1997).
20. Masuda, H., Yada, K. & Osaka, A. Self-ordering of cell configuration of anodic porous alumina with large-size pores in phosphoric acid solution. *Jpn. J. Appl. Phys.* **37,** L 1340-L 1342 (1998).
21. Nielsch, K., Choi, J., Schwirn, K., Wehspohn, R. B. & Gösele, U. Self-ordering regimes of porous alumina: The 10% porosity rule. *Nano Lett.* **2,** 677–680 (2002).
22. Lee, W. & Park, J. S. Porous anodic aluminum oxide: Anodization and templated synthesis of functional nanostructures. *Chem. Rev.* **114,** 7487–7556 (2014).
23. Santos, A., Kumeria, T. & Losic, D. Nanoporous anodic aluminum oxide for chemical sensing and biosensors. *TrAC, Trends Anal. Chem.* **44,** 25–38 (2013).

24. Santos, A., Kumeria, T. & Losic, D. Nanoporous anodic alumina: A versatile platform foro ptical biosensors. *Materials* **7,** 4297–4320 (2014).
25. Santos, A., Kumeria, T., Wang, Y. & Losic, D. *In situ* monitored engineering of inverted nanoporous anodic alumina funnels: On the precise generation of 3D optical nanostructures. *Nanoscale* **6,** 9991–9999 (2014).
26. Santos, A. *et al.* Nanoporous anodic alumina barcodes: Toward smart optical biosensors. *Adv. Mater.* **24,** 1050–1054 (2012).
27. Kumeria, T. *et al.* Structural and optical nanoengineering of nanoporous anodic alumina rugate filters for real-time and label-free biosensing applications. *Anal. Chem.* **86,** 1837–1844 (2014).
28. Kumeria, T. *et al.* Nanoporous anodic alumina rugate filters for sensing of ionic mercury: Toward environmental point-of-analysis systems. *ACS Appl. Mater. Interfaces* **6,** 12971–12978 (2014).
29. Kumeria, T. *et al.* Advanced structural engineering of nanoporous photonic structures: Tailoring nanopore architecture to enhance sensing properties. *ACS Photonics* **1,** 1298–1306 (2014).
30. Kumeria, T., Santos, A. & Losic, D. Nanoporous anodic alumina platforms: Engineered surface chemistry and structure for optical sensing applications. *Sensors* **14,** 11878–11918 (2014).
31. Kumeria, T., Santos, A. & Losic, D. Ultrasensitive nanoporous interferometric sensor for label-free detection of gold(III) ions. *ACS Appl. Mater. Interfaces* **5,** 11783–11790 (2013).
32. Rahman, M. M., Marsal, L. F., Pallarès, J. & Ferré-Borrull, J. Tuning the photonic stop bands of nanoporous anodic alumina-based distributed Bragg reflectors by pore widening. *ACS Appl. Mater. Interfaces* **5,** 13375–13381 (2013).
33. Shang, G. L. *et al.* Preparation of narrow photonic bandgaps located in the near infrared region an their applications in ethanol gas sensing. *J. Mater. Chem. C* **1,** 5285–5291 (2013).
34. Wang, B., Fei, G. T., Wang, M., Kong, M. G. & Zhang, L. D. Preparation of photonic crystals made of air pores in anodic alumina. *Nanotechnology* **18,** 365601 (2007).
35. Dronov, R., Jane, A., Shapter, J. G., Hodges, A. & Voelcker, N. H. Nanoporous alumina-based interferometric transducers ennobled. *Nanoscale* **3,** 3109–3114 (2011).
36. Yisen, L., Yi, C., Zhiyuan, L., Xing, H. & Yi, L. Structural coloring of aluminum. *Electrochem. Commun.* **13,** 1336–1339 (2011).
37. Li, J., Liang, G., Zhu, X. & Yang, S. Exploiting nanoroughness on holographically patterned three-dimensional photonic crystals. *Adv. Funct. Mater.* **22,** 2980–2986 (2012).
38. Ishizaki, T. & Sakamoto, M. Facile formation of biomimetic color-tuned superhydrophobic magnesium alloy with corrosion resistance. *Langmuir* **27,** 2375–2381 (2011).
39. Huang, Y. F., Jen, Y. J., Chen, L. C., Chen, K. H. & Chattopadhyay, S. Design for approaching cicada-wing reflectance in low- and high-index biomimetic nanostructures. *ACS Nano* **9,** 301–311 (2015).
40. Feng, L. *et al.* The structural color of red rose petals and their duplicates. *Langmuir* **26,** 14885–14888 (2010).
41. Yao, Z., Zhen, M., Ma, L. & Shen, W. The fabrication of ordered nanoporous metal films based on high field anodic alumina and their selected transmission enhancement. *Nanotechnology* **19,** 465705 (2008).
42. Santos, A., Formentín, P., Ferré-Borrull, J., Pallarès, J. & Marsal, L. F. Nanoporous anodic alumina obtained without protective oxide layer by hard anodization. *Mater. Lett.* **67,** 296–299 (2012).
43. Wang, Y., Santos, A., Evdokiou, A. & Losic, D. Rational design of ultra-short anodic alumina nanotubes by short-time pulse anodization. *Electrochim. Acta* **154,** 379–386 (2015).
44. Link, J. R. & Sailor, M. J. Smart dust: Self-assembling, self-orientating photonic crystals of porous Si. *Proc. Natl. Acad. Sci. USA.* **100,** 10607–10610 (2003).
45. Schmedake, T. A., Cunin, F., Link, J. R. & Sailor, M. J. Standoff detection of chemicals using porous silicon "smart dust" particles. *Adv. Mater.* **14,** 1270–1272 (2002).
46. Meade, S. O., Yoon, M. S., Ahn, K. H. & Sailor, M. J. Photonic silicon photonic crystals as encoded microcarriers. *Adv. Mater.* **16,** 1811–1814 (2004).
47. Cunin, F. *et al.* Biomolecular screening with encoded porous-silicon photonic crystals. *Nat. Mater.* **1,** 39–41 (2002).
48. Meade, S. O., Chen, M. Y., Sailor, M. J. & Miskelly, G. M. Multiplexed DNA detection using spectrally encoded porous SiO_2 photonic crystals particles. *Anal. Chem.* **81,** 2618–2625 (2009).
49. Dorvee, J. R., Derfus, A. M., Bhatia, S. N. & Sailor, M. J. Manipulation of liquid droplets using amphiphilic, magnetic one-dimensional photonic crystal chaperones. *Nat. Mater.* **3,** 896–899 (2004).
50. Wu, E. C. *et al.* Real-time monitoring of sustained drug release using the optical properties of porous silicon photonic crystal particles. *Biomaterials* **32,** 1957–1966 (2011).
51. Md Jani, A. M., Kempson, I. M., Losic, D. & Voelcker, N. H. Dressing in layers: Layering surface functionalities in nanoporous aluminum oxide membranes. *Angew. Chem., Int. Ed.* **49,** 7933–7937 (2010).
52. Abràmoff, M. D., Magalhaes, P. J. & Ram, S. J. Image processing with ImageJ. *Biophotonics Int.* **11,** 36–42 (2004).

Acknowledgements

Author Contributions

A.S. conceived the experiments. Y.C. and A.S. conducted the experiments. All authors analysed the results and reviewed the manuscript.

Additional Information

Supplementary information accompanies this paper at http://www.nature.com/srep

Competing financial interests: The authors declare no competing financial interests.

How to cite this article: Chen, Y. *et al.* Rational Design of Photonic Dust from Nanoporous Anodic Alumina Films: A Versatile Photonic Nanotool for Visual Sensing. *Sci. Rep.* **5**, 12893; doi: 10.1038/srep12893 (2015).